

# Interpolating between pair-potential systems

Lorenzo Costigliola,<sup>\*</sup> Andreas C. Martine, Claudia X. Romero, Jone E. Steinhoff,  
Francisco M. F. A. S. da Fonseca, Maria B. T. Nielsen, and Jeppe C. Dyre<sup>†</sup>  
*Glass and Time, IMFUFA, Department of Science and Environment,  
Roskilde University, P.O. Box 260, DK-4000 Roskilde, Denmark*  
(Dated: May 12, 2025)

This paper studies liquid-model systems with almost identical constant-potential-energy hypersurfaces. We simulated continuous interpolations between such systems, specifically between the Lennard-Jones (LJ), Weeks-Chandler-Andersen (WCA), exponent 12 inverse-power-law (IPL), and Yukawa (YK) pair-potential systems. Structure and dynamics were monitored via the radial distribution function and the time-dependent mean-square displacement, respectively. In terms of the interpolation parameter,  $0 \leq \lambda \leq 1$ , we argue that two systems have very similar constant-potential-energy hypersurfaces if the potential energies of configurations rarely cross when plotted as functions of  $\lambda$ . Such absence of “level crossing” applies to a very good approximation for the LJ to WCA transformation, and it also applies to a quite good approximation for the LJ to IPL and the YK to YK transformations (the latter varies the screening length). In all cases, structure and dynamics are shown to be almost invariant as functions of  $\lambda$ . The density is kept constant when  $\lambda$  is varied. Temperature must be generally adjusted with  $\lambda$ , which is done by an iterative “reduced-force-matching” method with no free parameters. We also apply the interpolation strategy to two versions of the Kob-Andersen (KA) binary LJ system and show that a recently introduced shifted-force-cutoff version of this system has constant-potential-energy hypersurfaces, which are almost identical to those of the original KA system. This result rationalizes the previously established fact that the two KA versions have virtually identical physics.

arXiv:2505.05656v1 [cond-mat.soft] 8 May 2025

---

<sup>\*</sup> lorenzo.costigliola@gmail.com

<sup>†</sup> dyre@ruc.dk

## I. INTRODUCTION

The simplest model liquids are described by Newtonian dynamics and involve only pair-potential interactions [1, 2]. Standard examples include the Lennard-Jones (LJ), inverse-power-law (IPL), and Yukawa (YK) pair-potential systems. It is always of interest when different systems have the same – or almost the same – structure and dynamics [2–10]. A classical example of this is the observation that the radial distribution function of the LJ system is very close to that of the hard-sphere system, an intriguing fact that was noted in 1968 in some of the earliest scientific computer simulations [11] and which inspired the advent of successful perturbation theories based on the hard-sphere system as the zeroth-order approximation [1, 2, 12–17].

The term “quasiuniversality” describes the fact that many pair-potential systems have very similar structure and dynamics [10]. This is usually rationalized by reference to the hard-sphere system: whenever two systems at two thermodynamic state points are described well by hard-sphere systems of the same packing fraction, the two systems have very similar physics. Incidentally, this reasoning was the background of Rosenfeld’s “excess-entropy scaling” principle from 1977 [18], which utilized the fact that the excess entropy is in a one-to-one correspondence with the packing fraction of the hard-sphere system mimicking the system in question. A recent alternative justification of quasiuniversality approximates the relevant pair potential as a sum of EXP (exponential repulsive) pair potentials [19]; by reference to isomorph theory [20–22] such a sum leads to approximately the same structure and dynamics as that of a single EXP pair-potential system [10, 23].

In this paper, which builds on ideas of Ref. 24, we take an alternative approach to predicting when one can expect two model liquids to have similar physics that does not introduce a reference system. Our main proposition is that this is the case whenever their constant-potential-energy hypersurfaces,  $\Omega$ , are almost identical [24]. If this applies, geodesic motion on the two  $\Omega$ s will be very similar. Since geodesic motion defines the so-called *NVU* dynamics that leads to the same physics as standard Newtonian dynamics [25, 26], the two systems must have very similar structure and dynamics.

We study below continuous interpolations between well-known pair-potential systems, which is implemented by introducing a parameter  $\lambda$  that varies from zero to unity. The investigation is divided into two parts. The first part shows results from computer simulations interpolating between different single-particle systems (Sec. III and Sec. IV), and a subsequent section studies an interpolation between two binary systems (Sec. V). In all cases we find that the constant-potential-energy hypersurface is almost independent of  $\lambda$  and that structure and dynamics, as predicted [24], are almost invariant with changing  $\lambda$ . In particular, this validates the above-mentioned *NVU*-based approach to the quasiuniversality of simple liquids [24]. The method used below is easily generalized to systems characterized by the non-spherically-symmetric interactions required to model molecular liquids.

## II. DETERMINING WHEN DIFFERENT SYSTEMS HAVE SIMILAR PHYSICS

Consider a system of  $N$  point particles described by classical mechanics. The system’s potential energy is denoted by  $U(\mathbf{R})$  in which  $\mathbf{R} = (\mathbf{r}_1, \dots, \mathbf{r}_N)$  where  $\mathbf{r}_i$  is the position vector of particle  $i$ . At a thermodynamic state point of temperature  $T$ , volume  $V$ , and (number) density  $\rho = N/V$ , the average potential energy is denoted by  $\langle U \rangle$ . The  $3N - 1$  dimensional *constant-potential-energy hypersurface*  $\Omega$  is then defined by

$$\Omega = \{\mathbf{R} \in \mathbb{R}^{3N} | U(\mathbf{R}) = \langle U \rangle\}. \quad (1)$$

We regard the collective position vector  $\mathbf{R}$  as a point on a hypersurface of this kind. Usually one assumes periodic boundary conditions, in which case  $\mathbb{R}^{3N}$  in Eq. (1) is replaced by a  $3N$ -dimensional torus (periodic boundary conditions are used throughout this paper). For simplicity, the discussion is limited to interpolations between systems of same density but generalization to systems of different densities is straightforward.

*NVU* dynamics is defined by replacing Newton’s equation of motion by geodesic motion on  $\Omega$ . This can be shown to not change the structure and dynamics of the system in question [25, 26]. For instance, the time-autocorrelation functions of *NVU* dynamics are identical to those of standard *NVE* or *NVT* dynamics (with obvious exceptions like the potential-energy time-autocorrelation function). As a consequence, if two systems have the same  $\Omega$  – possibly at state points with different temperatures – then they will have the same physics. Likewise, if they have *approximately* same  $\Omega$ , the physics will be *approximately* the same. By “same physics” we here mean same structure and dynamics while, e.g., thermodynamic properties like the average potential energy or the Helmholtz and Gibbs free energies are not expected to be identical (or even close). Note, however, that since the excess entropy is determined by the “volume” (area) of  $\Omega$  – specifically its logarithm [24] – this particular thermodynamic quantity *is* invariant whenever  $\Omega$  is.

The mathematical criterion for two systems, “0” and “1”, to have identical constant-potential-energy hypersurfaces is that for all configurations  $\mathbf{R}_a$  and  $\mathbf{R}_b$

$$U_0(\mathbf{R}_a) = U_0(\mathbf{R}_b) \implies U_1(\mathbf{R}_a) = U_1(\mathbf{R}_b). \quad (2)$$

The arrow  $\implies$  here represents a logical implication in the mathematical understanding of this term. By symmetry,  $\implies$  may be replaced by  $\iff$ . In practice, Eq. (2) is never rigorously obeyed for any two different systems. For this reason, it is more practical to be able to investigate whether two systems have *approximately* the same  $\Omega$  by replacing the equality sign in Eq. (2) by  $\cong$ . This requires quantifying to which degree  $\cong$  applies, however. An operational approach to check for approximately the same  $\Omega$  is to study to which degree the following implication applies

$$U_0(\mathbf{R}_a) < U_0(\mathbf{R}_b) \implies U_1(\mathbf{R}_a) < U_1(\mathbf{R}_b). \quad (3)$$

By going through the three different possibilities  $U_0(\mathbf{R}_a) < U_0(\mathbf{R}_b)$ ,  $U_0(\mathbf{R}_a) = U_0(\mathbf{R}_b)$ , and  $U_0(\mathbf{R}_a) > U_0(\mathbf{R}_b)$ , it is straightforward to show that Eq. (2) and Eq. (3) are mathematically equivalent. When it comes to numerical implementation, however, it makes better sense to check Eq. (3) than Eq. (2) for being approximately obeyed [27] (when is an equality sign almost obeyed?).

What are the requirements on  $U(\mathbf{R})$  in Eq. (2) and Eq. (3)? These criteria are no more restrictive than the general requirement of thermodynamic consistency, i.e., that the system in question has a well-defined bulk thermodynamic limit and, e.g., does not collapse with time. Exact mathematical criteria ensuring this were formulated long ago by Fisher and Ruelle [28, 29]. They showed that if the spatial integral of the pair potential is negative, the system is unstable. This implies that if  $U_0(\mathbf{R})$  is stable, a system with potential-energy function  $-U_0(\mathbf{R})$  is unstable. Thus one cannot use in Eq. (3)  $U_1(\mathbf{R}) = -U_0(\mathbf{R})$ , which would violate this condition but at the same time formally obey Eq. (2) by having the same constant-potential-energy hypersurface.

Below we investigate how well Eq. (3) applies by selecting a number of independent equilibrium configurations of system 0 and plotting how their potential energies change when the system is gradually transformed into system 1. If the curves generated in this way rarely cross, then Eq. (3) applies to a good approximation and the two  $\Omega$ s must be almost identical. Our approach is inspired by a similar procedure in isomorph theory [30], in which case it is the density of a given system that is changed, however, not the system itself.

As mentioned, we keep the density constant when comparing two systems. It is important to note that two systems may have the same  $\Omega$  at state points of same density but *different* temperatures. This is because the equilibrium temperature corresponding to a given  $\Omega$  is neither determined by the value of the potential energy on  $\Omega$  nor by the excess entropy  $S_{\text{ex}}$  (which quantifies the volume of  $\Omega$ ). Thus the temperature is given by the thermodynamic relation  $k_B T = (\partial U / \partial S_{\text{ex}})_\rho$  [20, 22, 24], which can differ even for two systems with same  $\Omega$ . Note that this issue is only encountered because we perform  $NVT$  simulations; the temperature does not need to be known if one instead uses  $NVU$  dynamics [25].

In order to check by  $NVT$  simulations whether two systems have the same – or very similar – physics, we need to determine the equilibrium temperature at a state point with the constant-potential-energy hypersurface  $\Omega$ . One way of doing this is by means of the so-called configurational temperature,  $T_{\text{conf}}$ , which in thermal equilibrium is identical to the temperature  $T$  and is defined [31–33] by

$$k_B T_{\text{conf}} \equiv \frac{\langle (\nabla U)^2 \rangle}{\langle \nabla^2 U \rangle}. \quad (4)$$

Here the sharp brackets denote canonical averages, which in the thermodynamic limit  $N \rightarrow \infty$  may be replaced by configuration-space microcanonical averages, i.e., averages over  $\Omega$ . In this limit, the relative fluctuations of  $(\nabla U)^2$  and  $\nabla^2 U$  actually go to zero, so for a large system one can estimate  $T_{\text{conf}}$  reliably from a single equilibrium configuration  $\mathbf{R} \in \Omega$ :

$$k_B T = k_B T_{\text{conf}} \cong k_B T_{\text{conf}}(\mathbf{R}) \equiv \frac{(\nabla U(\mathbf{R}))^2}{\nabla^2 U(\mathbf{R})}. \quad (5)$$

The relative error in this estimate decreases with system size as  $1/\sqrt{N}$ .

An alternative to using Eq. (5) for calculating the equilibrium temperature at a given state point is to employ so-called force matching [34]. This approach has the advantage that it does not involve the Laplacian of  $U$  but only forces, which are calculated anyway in a computer simulation. A disadvantage is that force matching in contrast to

Eq. (5) needs a reference system with same (or very similar)  $\Omega$  for which the temperature is known. If such a system is at hand, one can calculate the ratio of the temperature of the system in question to that of the reference system from the following argument referring to the thermodynamic limit (for details please see Refs. 24 and 34): At any point  $\mathbf{R}$  on  $\Omega$ , the normal vector  $\mathbf{n}(\mathbf{R})$  is given by  $\mathbf{n}(\mathbf{R}) = \nabla U(\mathbf{R})/|\nabla U(\mathbf{R})|$ . The curvature  $\kappa(\mathbf{R})$ , which expresses how fast the normal vector changes when moving on  $\Omega$ , is given [24] by  $\kappa(\mathbf{R}) \propto \nabla \cdot \mathbf{n}(\mathbf{R}) \cong \nabla^2 U(\mathbf{R})/|\nabla U(\mathbf{R})| \cong |\mathbf{F}(\mathbf{R})|/T_{\text{conf}}(\mathbf{R})$  in which  $\mathbf{F}(\mathbf{R}) = -\nabla U(\mathbf{R})$  is the  $3N$ -dimensional force vector and  $\cong$  signals that the relative deviations vanish in the thermodynamic limit. The equilibrium temperature  $T$  of the system in question relative to that of the reference system,  $T_0$ , is determined by the fact that since the two systems have the same  $\Omega$ , one has  $\kappa = \kappa_0$  implying that

$$T = T_0 \frac{|\mathbf{F}(\mathbf{R})|}{|\mathbf{F}_0(\mathbf{R})|}. \quad (6)$$

We refer to Eq. (6) as “reduced-force matching”; the determination of  $T$  according to this is carried out iteratively (Appendix). We note that, except for a density factor that is the same in all cases of this paper, the quantity  $\mathbf{F}(\mathbf{R})/k_B T$  is the so-called reduced force that plays an important role in isomorph theory [20–22].

### III. PAIR POTENTIALS AND SIMULATION DETAILS

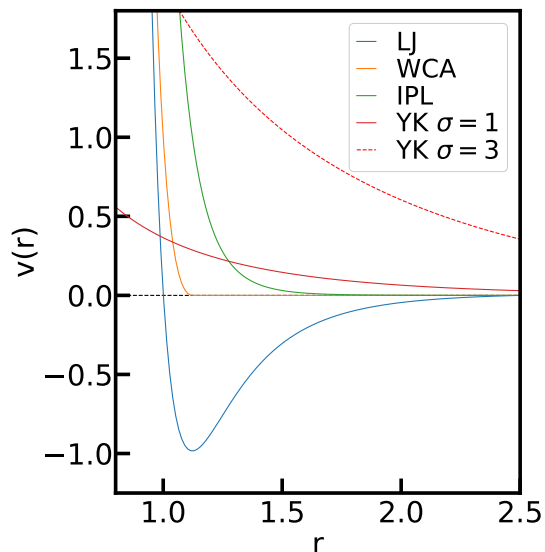


FIG. 1. The pair potentials studied. Plotted as functions of the pair distance  $r$ , the figure shows the Lennard-Jones (LJ), Weeks-Chandler-Andersen (WCA), inverse power-law with exponent 12 (IPL), and Yukawa (YK) pair potentials. The Yukawa potential is shown for two characteristic lengths,  $\sigma = 1$  and  $\sigma = 3$ , between which we extrapolate (Fig. 5).

We consider a systems of  $N \gg 1$  particles of same mass,  $m$ . If  $r_{ij}$  is the distance between particles  $i$  and  $j$ , in terms of the pair potential  $v(r)$  the total potential energy  $U$  is given by  $U(\mathbf{R}) = \sum_{i < j} v(r_{ij})$ . This paper considers some of the most commonly studied pair potentials, the Lennard-Jones [35], Weeks-Chandler-Andersen [12], inverse-power-law with exponent 12 [6, 36–38], and Yukawa [39] potentials (Fig. 1). These are defined by

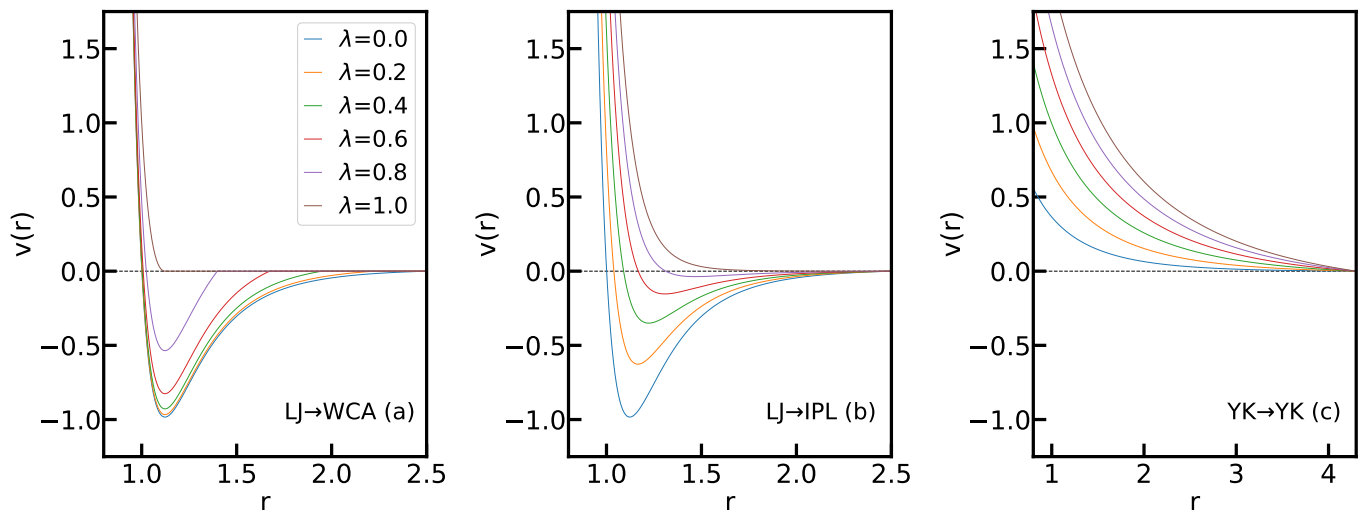


FIG. 2. The three simulated pair-potential interpolations, each of which is shown for six values of  $\lambda$  (legend of (a)). (a) LJ  $\rightarrow$  WCA, corresponding to cut-and-shifted LJ systems with a cutoff that decreases from 2.5 ( $\lambda = 0$ , defining the standard LJ system) to  $2^{1/6}$  ( $\lambda = 1$ , defining the WCA system); (b) LJ  $\rightarrow$  IPL; (c) YK  $\rightarrow$  YK. In all cases the potentials vary significantly so *a priori* one might expect quite different physics.

$$\begin{aligned}
 v_{\text{LJ}}(r) &= 4\varepsilon \left( (r/\sigma)^{-12} - (r/\sigma)^{-6} \right) \\
 v_{\text{WCA}}(r) &= \begin{cases} v_{\text{LJ}}(r) - v_{\text{LJ}}(2^{1/6}\sigma), & r < 2^{1/6}\sigma \\ 0, & r > 2^{1/6}\sigma \end{cases} \\
 v_{\text{IPL}}(r) &= \varepsilon (r/\sigma)^{-12} \\
 v_{\text{YK}}(r) &= \frac{\varepsilon}{(r/\sigma)} e^{-r/\sigma}.
 \end{aligned} \tag{7}$$

In these expressions  $\varepsilon$  determines the energy scale and  $\sigma$  the length scale of the pair interaction. Unless otherwise stated we use the rationalized unit system in which  $\varepsilon = 1$ ,  $\sigma = 1$ , and  $k_B = 1$ . When evaluating how much structure and dynamics vary when interpolating between two pair potentials, the density  $\rho$  is kept constant while temperature is adjusted as described in Sec. II and the Appendix.

A general method of interpolating between system 0 of pair potential  $v^{(0)}(r)$  and system 1 of pair potential  $v^{(1)}(r)$  uses the convex combination  $v^{(\lambda)}(r) = (1 - \lambda)v^{(0)}(r) + \lambda v^{(1)}(r)$  ( $0 \leq \lambda \leq 1$ ), a one-parameter family of pair potentials that clearly interpolates smoothly between systems 0 and 1. Below we take this approach in some cases, but generally employ the philosophy of implementing the interpolations in the most natural way. In this connection, recall that in their 1971 paper [12], Weeks, Chandler, and Andersen regarded the LJ pair potential as a sum of a purely repulsive (“WCA”) and an attractive term, which suggests that an obvious way of interpolating from LJ to WCA by gradually removing the attractive term. We instead utilize the fact that the WCA pair potential is defined as the LJ pair potential, cut and shifted at the potential-energy minimum, and gradually reduce the cutoff from the standard  $r_c = 2.5$  to  $r_c = 2^{1/6}$  that identifies the LJ pair-potential minimum.

All simulations were carried out using the GPU-optimized Molecular Dynamics code RUMD [40] with standard Nose-Hoover  $NVT$  dynamics [41]. For the single-component systems  $N = 4096$  particles were simulated, for the binary systems  $N = 4000$ , in both cases at typical liquid state points. More details about the simulations are given in the Appendix.

#### IV. INTERPOLATING BETWEEN SINGLE-PARTICLE SYSTEMS

We transform LJ gradually into WCA, denoted by LJ  $\rightarrow$  WCA, by reducing the standard shifted-potential cutoff from 2.5 to  $2^{1/6}$ , i.e.,

$$v_{\text{LJ} \rightarrow \text{WCA}}^{(\lambda)}(r) = \begin{cases} v_{\text{LJ}}(r) - v_{\text{LJ}}(r_c(\lambda)) & , r < r_c(\lambda) \equiv (1 - \lambda)2.5 + \lambda 2^{1/6} \\ 0 & , r > r_c(\lambda). \end{cases} \quad (8)$$

Clearly,  $v_{\text{LJ} \rightarrow \text{WCA}}^{(0)}(r) = v_{\text{LJ}}(r)$  with a shifted-potential cutoff at 2.5 and  $v_{\text{LJ} \rightarrow \text{WCA}}^{(1)}(r) = v_{\text{WCA}}(r)$ .

The second interpolation is between LJ and IPL, which is carried out by gradually removing the attractive  $r^{-6}$  term:

$$v_{\text{LJ} \rightarrow \text{IPL}}^{(\lambda)}(r) = 4 (r^{-12} - (1 - \lambda)r^{-6}). \quad (9)$$

This expression has the required limits  $v_{\text{LJ} \rightarrow \text{IPL}}^{(0)}(r) = 4(r^{-12} - r^{-6})$  and  $v_{\text{LJ} \rightarrow \text{IPL}}^{(1)}(r) = 4r^{-12}$ .

The third case interpolates between two Yukawa pair potentials of different screening length. This is done by changing the parameter  $\sigma$  in Eq. (7) from 1 to 3, i.e., by putting  $\sigma = 1 + 2\lambda$ :

$$v_{\text{YK} \rightarrow \text{YK}}^{(\lambda)}(r) = \frac{1 + 2\lambda}{r} e^{-r/(1+2\lambda)}. \quad (10)$$

Figure 2 shows the pair potentials of these interpolations for six values of  $\lambda$ . We note that the pair potentials vary considerably with  $\lambda$ .

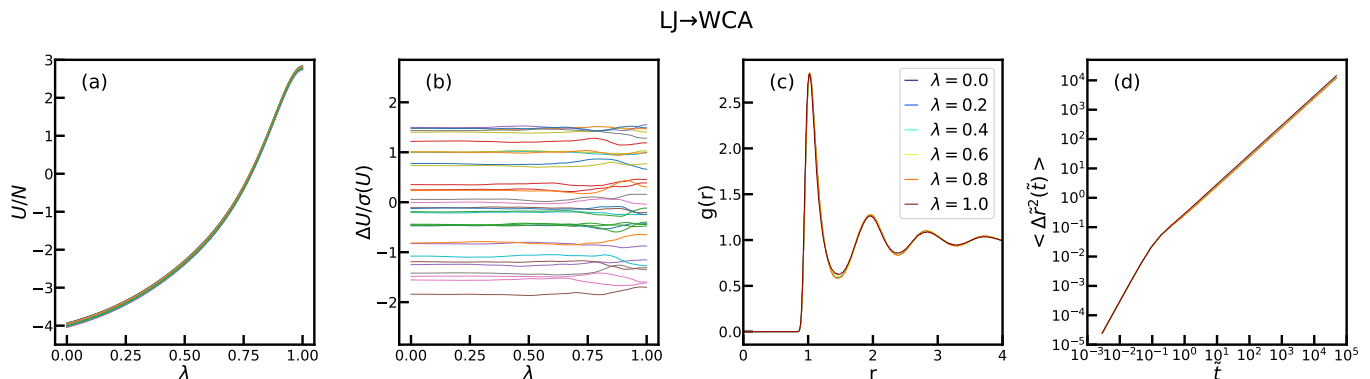


FIG. 3. Results for the LJ  $\rightarrow$  WCA interpolation. The reference state point  $(\rho, T) = (1.0, 2.0)$  is where the  $\lambda = 0$  simulation was carried out, which forms the basis for the  $\lambda$ -scaling plots in (a) and (b). (a) Per-particle potential energy with changing  $\lambda$  plotted for 32 independent configurations. (b) Fluctuations of  $U$  around the sample-average for 32 independent configurations, scaled with the standard deviation  $\sigma(U)$ . For  $\lambda < 0.75$  there are virtually no “level crossings”, and for  $\lambda > 0.75$  Eq. (3) is still largely obeyed. (c) Radial distribution functions  $g(r)$  for six  $\lambda$  values. For each  $\lambda$  the temperature was adjusted according to the reduced-force-matching criterion Eq. (6), leading only to minor temperature changes (see below). (d) Reduced-unit mean-square displacement as a function of time with changing  $\lambda$ .

Consider first LJ  $\rightarrow$  WCA (Fig. 3). Panel (a) shows how the potential energy varies with  $\lambda$  for 32 independent configurations generated in a standard equilibrium Nose-Hoover  $NVT$  simulation of the LJ system (defining  $\lambda = 0$ ) at the reference thermodynamic state point  $(\rho, T) = (1.0, 2.0)$ . No extra simulations were carried out in order to calculate how the potential energies of these configurations change with  $\lambda$ , which is determined entirely by the pair potential  $v_{\text{LJ} \rightarrow \text{WCA}}^{(\lambda)}(r)$  and the configuration in question. Not surprisingly, the potential energy increases when the shifted-potential cutoff is reduced; in fact it changes from negative to positive values. It is not possible to judge from panel (a) to which degree Eq. (3) is obeyed, however, because the potential energies of the 32 configurations follow each other closely. To investigate the Eq. (3) criterion we plot in panel (b) the normalized potential-energy variation,  $\Delta U/\sigma(U)$ , in which  $\Delta U = U - \langle U \rangle$  and  $\sigma^2(U) \equiv \langle (\Delta U)^2 \rangle = \langle U^2 \rangle - \langle U \rangle^2$  (averaging over the 32 configurations). If these curves never intersect – no “level crossings” – then Eq. (3) is rigorously obeyed. This is not rigorously the case, but it does apply to a very good approximation. Consequently, as argued above by reference to  $NVT$  dynamics, one expects very similar structure and dynamics. We investigate this by carrying out  $NVT$  simulations for  $\lambda = 0.0, 0.2, 0.4, 0.6, 0.8, 1.0$  (all at density 1.0), with temperatures adjusted by reduced-force matching (Sec. II and the Appendix). The resulting radial distribution function (RDF) and the reduced-unit mean-square displacement

(MSD) as a function of time are shown in panels (c) and (d). The structure and dynamics of all systems are clearly very similar. This is not at all unexpected in view of the well-known fact that the WCA system provides an excellent approximation to the LJ system [2, 12], which is further confirmed by the fact that the temperature adjustments all are below 5% (in fact, not adjusting the temperature gives virtually the same results).

The LJ  $\rightarrow$  IPL interpolation is studied in Fig. 4 at the same reference state point,  $(\rho, T) = (1.0, 2.0)$ . Although the IPL and LJ pair potentials are quite different, (b) shows that Eq. (3) is obeyed to a quite good approximation. Panels (c) and (d) show structure and dynamics at the temperature of the reference state point,  $T = 2.0$ , for varying  $\lambda$ . Panels (e) and (f) show analogous data with temperature adjustment, leading to almost perfect data collapse. We return to the magnitude of the temperature adjustment in Fig. 6 below.

We finally turn to YK  $\rightarrow$  YK, in which case the reference state point is  $(\rho, T) = (0.5, 0.02)$ . As previously, we performed a  $\lambda = 0$  simulation to generate the 32 configurations used to calculate the potential energies as functions of  $\lambda$  according to Eq. (10). Figure 5(a) shows that the potential energies of these configurations scale in a very similar way when  $\lambda$  is increased. Again, this does not allow for checking how well Eq. (3) applies. Panel (b) shows few level crossings. Indeed, structure and dynamics are almost independent of  $\lambda$  for the temperature-adjusted simulations (panels (e) and (f)), which is in notable contrast to what happens if temperature is not adjusted (panels (c) and (d)).

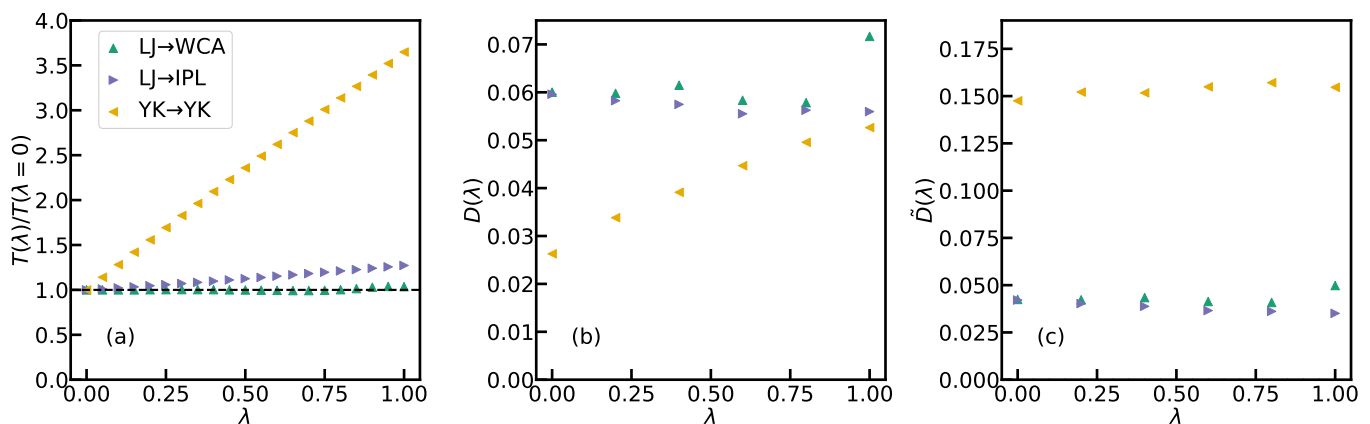


FIG. 6. Temperature adjustment. (a) shows the temperatures determined by reduced-force matching as functions of  $\lambda$  (the black dashed horizontal line marks unity). In the LJ  $\rightarrow$  WCA case the effect is very small, which confirms the well-known fact that the LJ and WCA systems have very similar physics at a given state point [12]. In the LJ  $\rightarrow$  IPL case up to 25% temperature adjustment is needed, and even larger adjustments are necessary for YK  $\rightarrow$  YK. (b) shows the diffusion coefficients  $D$  as a function of  $\lambda$  (obtained from the long-time MSD). (c) shows analogous data for the reduced diffusion coefficient  $\tilde{D}$  with the  $T(\lambda)$  temperature adjustment in the  $NVT$  simulation. The reduced diffusion coefficients are almost constant with changing  $\lambda$ .

For the three interpolations Fig. 6(a) shows the reduced-force-matching temperatures relative to the reference temperature. Figure 6(b) shows the variation with  $\lambda$  of the diffusion coefficient,  $D$ , and (c) shows how much the reduced diffusion coefficient defined by  $\tilde{D} \equiv \rho^{1/3} \sqrt{m/k_B T} D = \rho^{1/3} T^{-1/2} D$  [18, 20] varies with  $\lambda$  (the last equality reflects our use of rationalized units).  $\tilde{D}$  is almost constant. This confirms the invariance of the dynamics when temperature adjustment is implemented.

## V. INTERPOLATING BETWEEN TWO VERSIONS OF A BINARY LJ SYSTEM

In order to illustrate the generality of our method, this section studies a transformation involving the well-known Kob-Andersen (KA) binary LJ mixture [42]. The KA system, which consists of 80% A particles and 20% B particles, is resistant against crystallization and therefore easily supercooled [43, 44]. For this reason the KA system has become a standard model for simulation studies of glass-forming liquids [44–47]. Writing the LJ pair potential between particles of type  $\alpha$  and  $\beta$  as  $v_{\alpha\beta}(r) = 4\varepsilon_{\alpha\beta}((r/\sigma_{\alpha\beta})^{-12} - (r/\sigma_{\alpha\beta})^{-6})$ , in which  $\alpha$  is A or B and likewise for  $\beta$ , the parameters defining the KA system are [43]:  $\sigma_{AA} = 1.0$ ,  $\sigma_{AB} = \sigma_{BA} = 0.8$ ,  $\sigma_{BB} = 0.88$ ,  $\varepsilon_{AA} = 1.0$ ,  $\varepsilon_{AB} = \varepsilon_{BA} = 1.5$ ,  $\varepsilon_{BB} = 0.5$ .

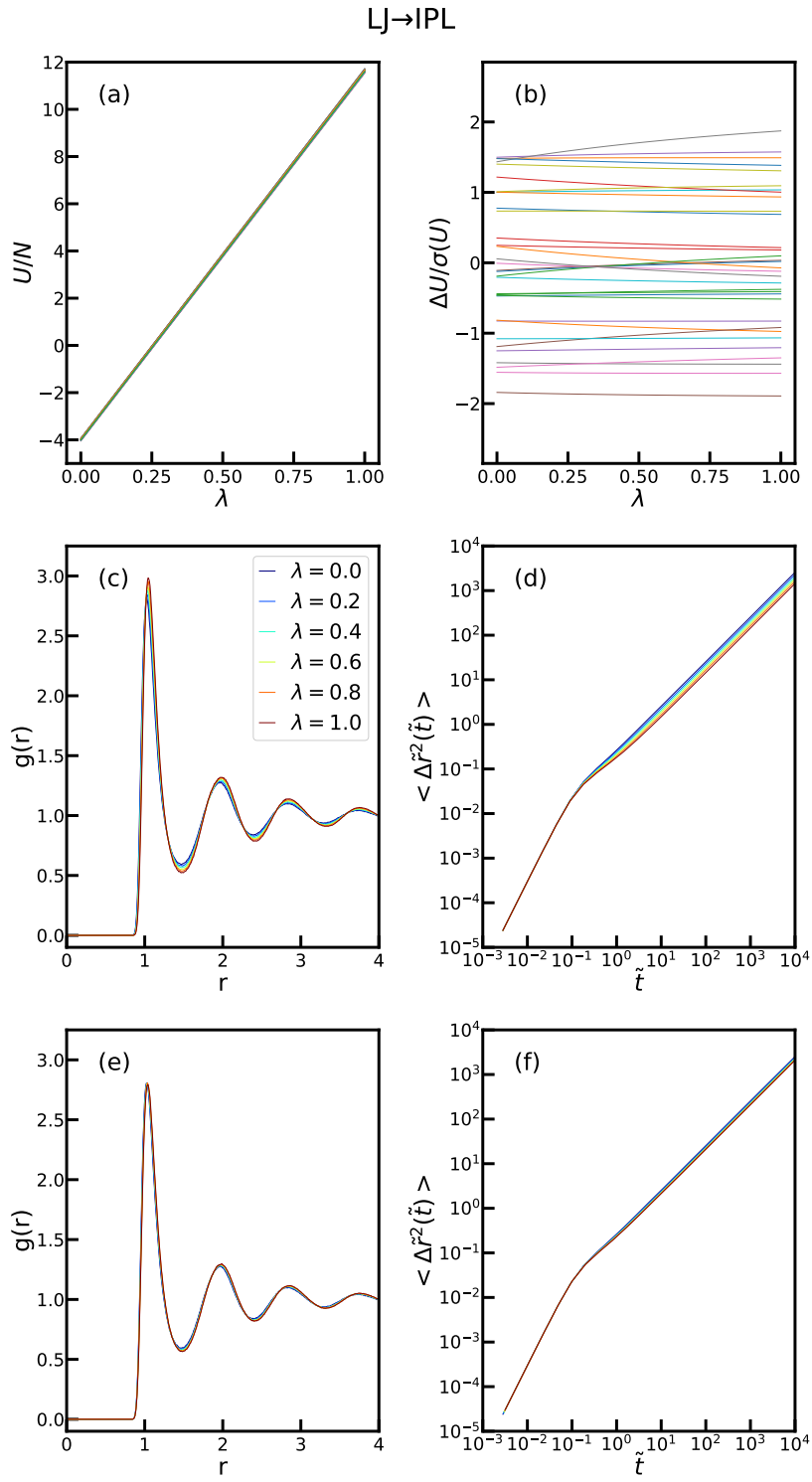


FIG. 4. Results for LJ  $\rightarrow$  IPL with reference state point  $(\rho, T) = (1.0, 2.0)$ . (a) and (b) are analogous to the same panels in Fig. 3. (c) and (d) show the variation of structure and dynamics if no temperature adjustment is implemented, in which case the physics is not quite invariant. (e) and (f) show structure and dynamics when the temperature is adjusted according to the reduced-force matching method (Appendix). Here both structure and dynamics are invariant to a much higher degree.

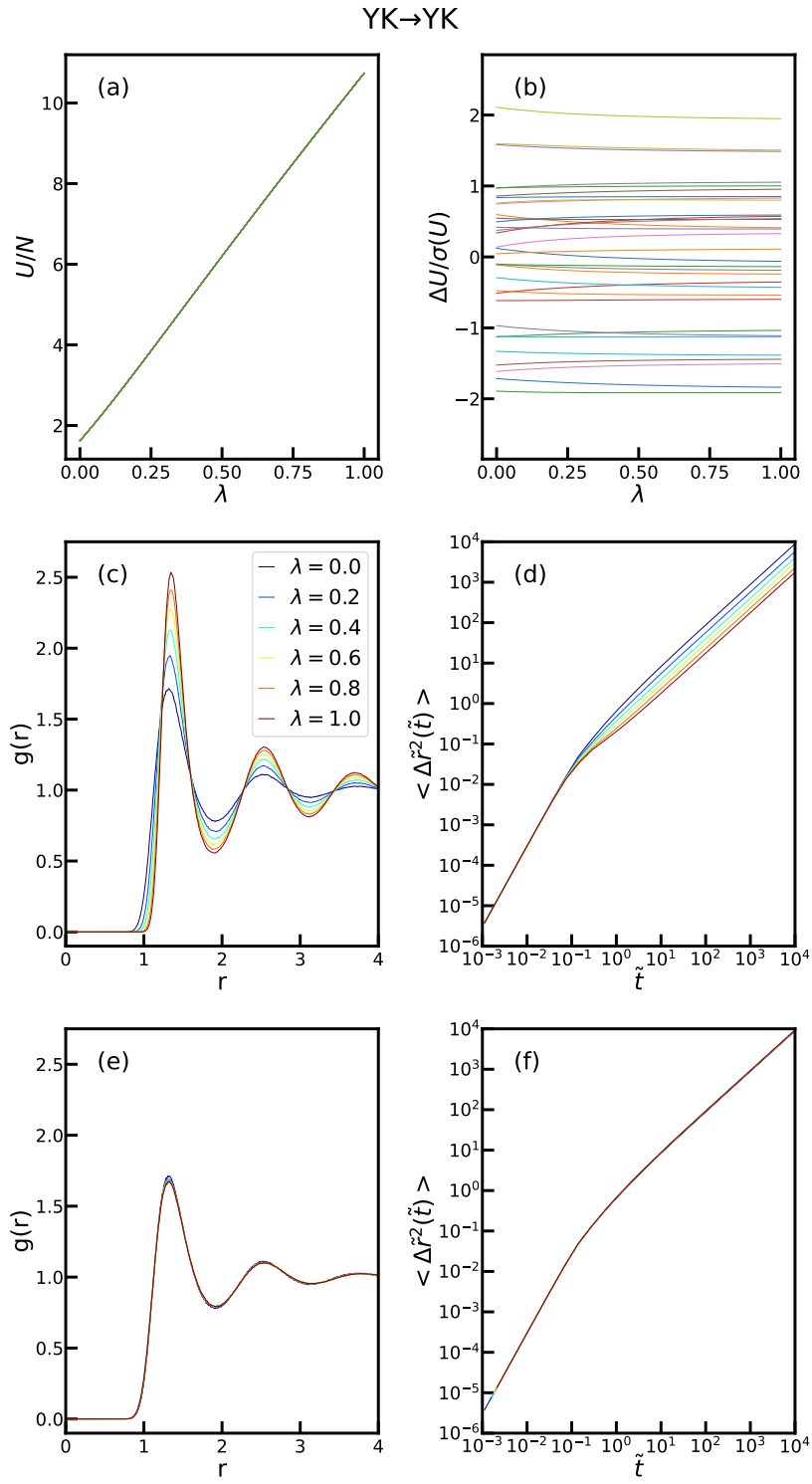


FIG. 5. Results for YK  $\rightarrow$  YK with reference state point  $(\rho, T) = (0.5, 0.02)$ . (a) and (b) are analogous to the same panels in Fig. 3. (c) and (d) show the structure and dynamics if no temperature adjustment is carried out. Clearly the physics changes a lot with  $\lambda$ . (e) and (f) show the same with temperature adjusted, in which case structure and dynamics are invariant to a good approximation.

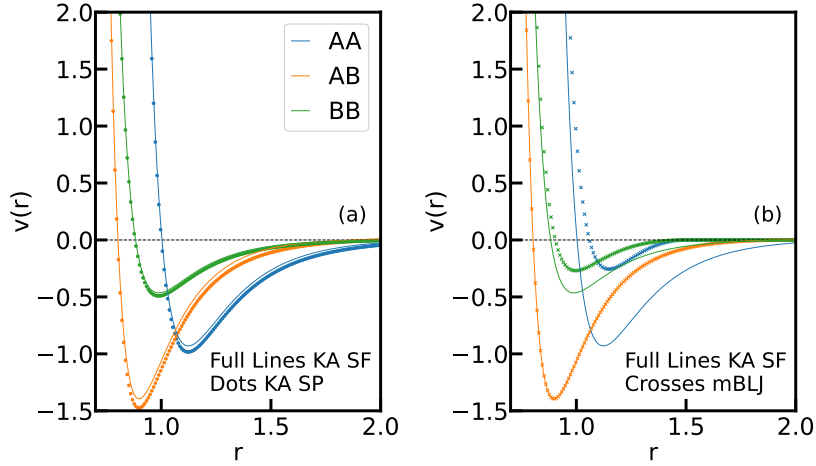


FIG. 7. Binary LJ pair potentials. (a) shows the potentials of the standard, shifted-potential (SP) cutoff version of the KA model (dots) and the shifted-force (SF) version with the same cutoffs (full curves). The two cases have almost the same pair potentials, which is a consequence of the relatively large cutoff used. (b) compares the SF version of the KA system with its modified version (mBLJ) that has significantly smaller like-particle cutoffs.

We interpolate between the standard KA model and a novel version of it, the so-called modified binary LJ (mBLJ) model that is at least 100 times less prone to crystallization [48]. This is achieved by changing the like-particle pair-potential cutoffs to shifted-force cutoffs at significantly smaller distances. Recall that a shifted-force cutoff at  $r_c$  replaces the pair force  $f(r) \equiv -v'(r)$  by  $f(r) - f(r_c)$  below  $r_c$  [41, 49], a procedure that results in much better energy conservation than the standard shifted-potential cutoff because the pair-force discontinuity at  $r_c$  is eliminated. In the present case, the primary effect of switching to short-range shifted-force cutoffs is that the like-particle attractive interactions become much weaker than in the standard KA model thus preventing crystallization of the KA system (which proceeds via phase separation and subsequent creation of a pure A particle face-centered cubic crystal [44]). Specifically, the mBLJ model has like-particle shifted-force cutoffs at  $r_c = 1.5\sigma_{AA}$ , while a shifted-force cutoff at  $r_c = 2.5\sigma_{AB}$  is used for the AB interaction.

The standard KA model involves cutoffs at  $r_c = 2.5\sigma_{\alpha\beta}$ . One usually implements these as shifted-potential cutoffs, but for technical reasons we use shifted-force cutoffs also to represent the standard KA model. The KA and mBLJ pair potentials with different cutoffs are shown in Fig. 7. Panel (a) compares the shifted-potential and shifted-force versions of the standard KA system of  $r_c = 2.5\sigma_{\alpha\beta}$  cutoffs. We see that there is little difference, and as shown in the Appendix the dynamics of the two systems are indeed very similar. This justifies our use of the shifted-force KA version as the  $\lambda = 0$  starting point for the extrapolation representing the standard KA model. Panel (b) shows the shifted-force KA and mBLJ pair potentials. The like-particle attractions are much weaker in the mBLJ case than in the KA case, in particular for the A particles.

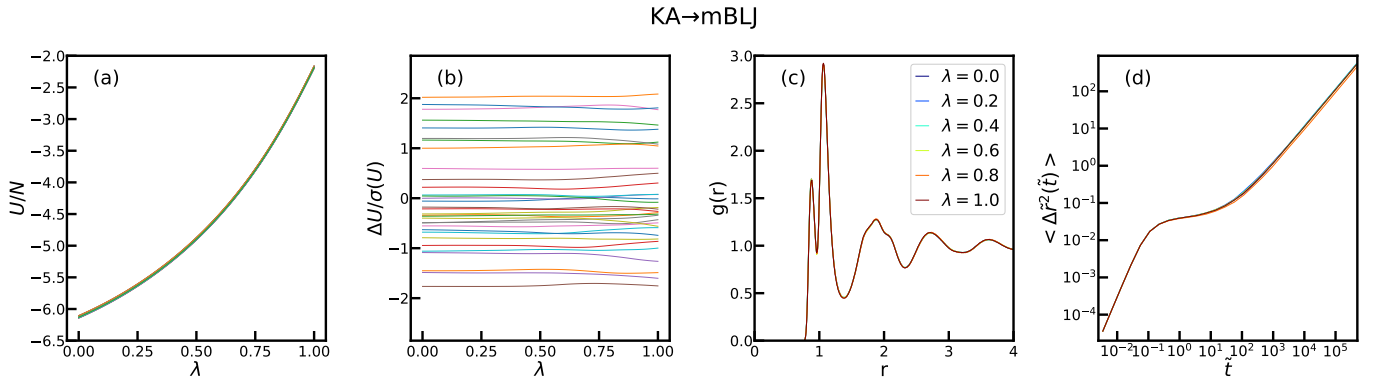


FIG. 8. Results for the binary system interpolation  $\text{KA} \rightarrow \text{mBLJ}$ , plotted as for the single-component interpolations. Just as in the single-component cases, the invariance of  $\Omega$  that is evident from (b) translates into invariance of the structure and the dynamics. (c) and (d) refer to all-particle data with temperature adjustment, i.e., the A and B particles are not distinguished here.

The interpolation from the standard KA model to the mBLJ model is carried out by using shifted-force cutoffs that are a convex combination of the old and new ones, i.e., for each of the three pair interactions the cutoff  $r_c(\lambda)$  is written as  $1 - \lambda$  times the KA cutoff plus  $\lambda$  times the mBLJ cutoff. For the like-particle interactions this amounts to  $r_c(\lambda) = (2.5 - \lambda)\sigma_{AA}$  for the A particles and  $r_c(\lambda) = 2.5(1 - \lambda)\sigma_{BB} + 1.5\lambda\sigma_{AA}$  for the B particles; for the AB interaction the cutoff remains at  $2.5\sigma_{AB}$ . Figure 8 shows the results of this transformation. The reference state point is  $(\rho, T) = (1.2, 0.48)$ , which is in the less-viscous liquid phase compared to the lower temperatures of current numerical studies of glass-forming liquids closer to the glass transition. As previously, panel (a) shows the potential-energy variation as a function of  $\lambda$  and (b) shows the relative variations. There are few level crossings. Consistent with this (c) and (d) show invariant (all-particle) structure and dynamics (temperature-adjusted data).

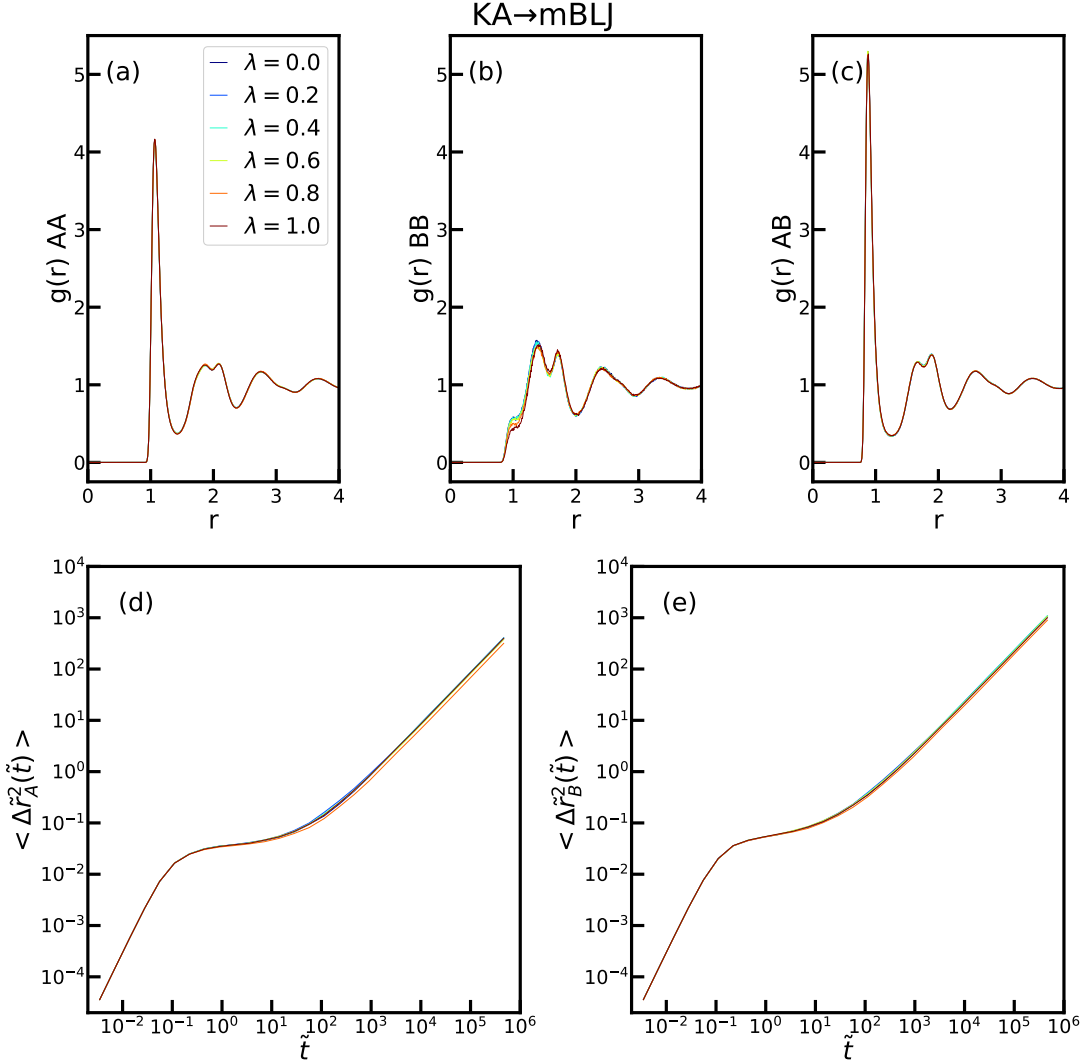
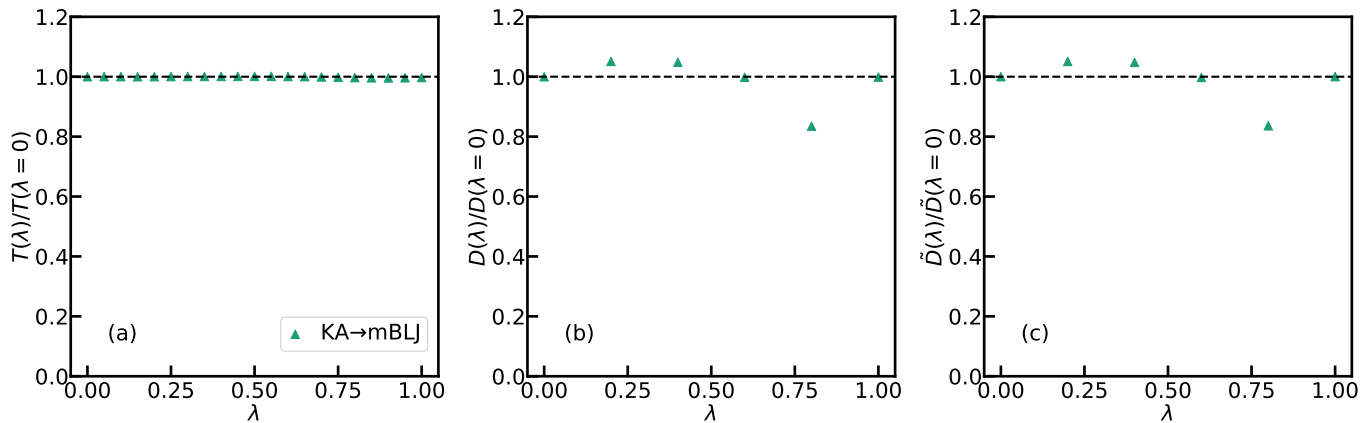


FIG. 9. Closer analysis of the KA  $\rightarrow$  mBLJ interpolation in which (a), (b), and (c) report RDF data while (d) and (e) report MSD data. Overall, there is good data collapse.

Given that the KA system consists of two different particle types, one may ask whether the structure and dynamics of A and B particles separately are invariant. This is investigated in Fig. 9. Overall we see good invariance.

TABLE I. Diffusion coefficient  $D$  as a function of  $\lambda$  (left column) for the four system considered.

$\lambda$	$D$			
	LJ $\rightarrow$ WCA	LJ $\rightarrow$ IPL	YK $\rightarrow$ YK	KA $\rightarrow$ mBLJ
0.00	0.0600	0.0596	0.0263	0.000129
0.20	0.0598	0.0583	0.0338	0.000135
0.40	0.0615	0.0575	0.0391	0.000135
0.60	0.0583	0.0555	0.0447	0.000128
0.80	0.0578	0.0563	0.0496	0.000107
1.00	0.0717	0.0560	0.0526	0.000128

FIG. 10. Effect of temperature adjustment in the KA  $\rightarrow$  mBLJ case. (a) shows that only very little adjustment is needed. (b) and (c) show data for the all particle diffusion coefficient and its reduced-unit version.

We finally show in Fig. 10(a) that virtually no temperature adjustment is needed in the KA  $\rightarrow$  mBLJ case. This important result is consistent with previous extensive simulations carried out at  $T = 0.37$  at which the system is strongly supercooled; here the KA and mBLJ systems were also found to have virtually the same dynamics [48]. The relative variation of the diffusion coefficient and its reduced version are shown in (b) and (c), respectively. There is little variation although we note a drop at  $\lambda = 0.8$  for which we have no explanation.

## VI. DISCUSSION

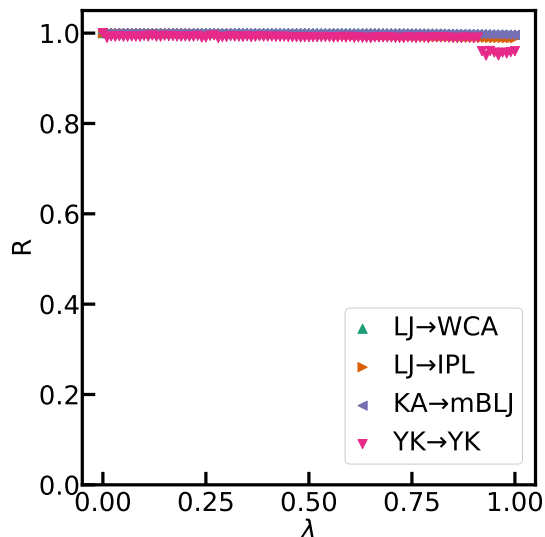


FIG. 11. Correlation coefficient  $R$  between the potential energies as a function of  $\lambda$ . Each point represents the Pearson correlation coefficient obtained by considering as independent variable the potential energies of the 32 configurations at  $\lambda = 0$  and as dependent variable the potential energies of the same 32 configurations evaluated at the  $\lambda$  values indicated. In all cases the correlations are very strong;  $R$  is mostly above 0.99 and always above 0.95.

This paper has studied gradual interpolations between some of the most commonly used pair-potential systems. We presented data for three interpolations between single-component pair-potential systems and data for an interpolation between two different versions of the KA binary LJ liquid. In all four cases there are only few “level crossings”, which means that Eq. (3) applies to a good approximation. This claim is a bit hand-waving, however. Can one quantify to how large a degree Eq. (3) is fulfilled? Inspired by Ref. 27 we use the Pearson correlation coefficient  $R$  between the 32 different potential energies at the starting point  $\lambda = 0$  and an arbitrary  $\lambda \leq 1$ . Figure 11 shows such data plotted with the ordinate axis going to zero in order to visualize how close the correlation coefficients are to unity. Most data have  $R > 0.99$ , but the YK  $\rightarrow$  YK interpolation has  $0.95 < R < 0.96$ . In summary, the intuitive criterion of “few” level crossings translates into correlation coefficients that are indeed close to unity.

Interpolation between two pair-potential systems was achieved by introducing a parameter  $\lambda$  such that system 0 corresponds to  $\lambda = 0$  and system 1 to  $\lambda = 1$ . The following criterion was used for checking whether two systems have the same, or almost the same, constant-potential-energy hypersurface  $\Omega$ : First one selects a number (here 32) of statistically independent equilibrium configurations of system 0 at the reference state point. If the potential energies of these configurations as functions of  $\lambda$  show no or only few level crossings, the two systems have the same or almost the same  $\Omega$ . By reference to the equivalence of  $NVU$  and  $NVT$  dynamics, this implies the same or almost the same structure and dynamics. The excess entropy  $S_{\text{ex}}$  is also the same or almost the same for the two systems, while other thermodynamic quantities like the potential energy and the Helmholtz and Gibbs free energies are not expected to be invariant when interpolating system 0 and system 1. We note, incidentally, that our findings confirm the quasuniversality of simple liquids [2–10] by the fact that all systems have almost identical  $\Omega$ , structure, and dynamics (compare Figs. 3-5 and 8).

An important point is that if two systems have the same  $\Omega$  at two state points of same density, this does not imply the two systems have the same temperature. A crucial ingredient of the interpolation method is therefore the introduction of iterative reduced-force matching based on Eq. (6), which identifies the temperature at which the  $\lambda$  system is predicted to have the same physics as system 0 at the reference state point.

We checked for “same physics” by evaluating the RDF and the MSD. An obvious question is whether more complex liquid characteristics like higher-order structural measures or collective dynamic quantities like the frequency-dependent viscosity are also expected to be (virtually) invariant if there are only few level crossings. We have not investigated this but do expect it to be the case because of the equivalence of  $NVU$  and  $NVT$  dynamics [25]. It would be interesting to have this confirmed by additional simulations. Another point it would be useful to look into in future works is the effect of changing the ratio of the A and B particle masses of the binary LJ system. Following the original Kob-Andersen paper [43] we assumed identical masses, but changing the ratio will modify both the single-particle

and the collective dynamics. At the same time, the above  $NVU$ -based arguments would not be affected because the statistical Boltzmann probability are not influenced by the particle masses. Our prediction is that one would still see very similar dynamics of the shifted-potential and shifted-force versions of the system, however. We base this expectation on the fact that standard  $NVU$  geodesic dynamics is modified for systems of different particle masses because the metric defining geodesics itself involves the particle masses, a point first discussed by Hertz [50, 51].

The interpolation approach introduced above is general. It is not limited to pair-potential systems or to systems of same density, although these two restrictions apply to the cases studied. For future work, in order to validate our “absence-of-level-crossing” criterion ensuring very similar structure and dynamics after temperature adjustment, it will be important to study systems of varying density [20, 22], as well as to interpolate between non-pair potential systems, between atomic and molecular models, and between different molecular models.

#### DATA AVAILABILITY

The repository <https://zenodo.org/records/15113178> contains the data discussed in this work and the Jupyter notebook used for producing the figures.

#### ACKNOWLEDGMENTS

The proof of concept for this work was established in a Roskilde University bachelor project by Ana Maria B. Brea, Andreas C. Martine, Claudia X. Romero, Jone E. Steinhoff, Francisco M. F. A. S. da Fonseca, Maria B. T. Nielsen, and Victor E. S. Rasmussen. The project was supervised by J.C.D. and L.C. After graduating, Martine, Romero, Steinhoff, da Fonseca, and Nielsen contributed to the writing of the paper. This work was supported by the VILLUM Foundation’s *Matter* grant VIL16515.

## APPENDIX

This Appendix gives further simulation details, compares the dynamics of the shifted-potential and shifted-force KA versions with same (long) cutoff, and describes the iterative reduced-force-matching method.

## Simulation details

All simulations were performed using the GPU-optimized Molecular Dynamics code RUMD [40] using an *NVT* integrator based on a leap-frog discretization of the Newtonian equation of motion coupled with a Nose-Hoover thermostat. Table I lists the number of steps "Short sim" and "Long sim" indicated as vertical dashed lines in Fig. A1.

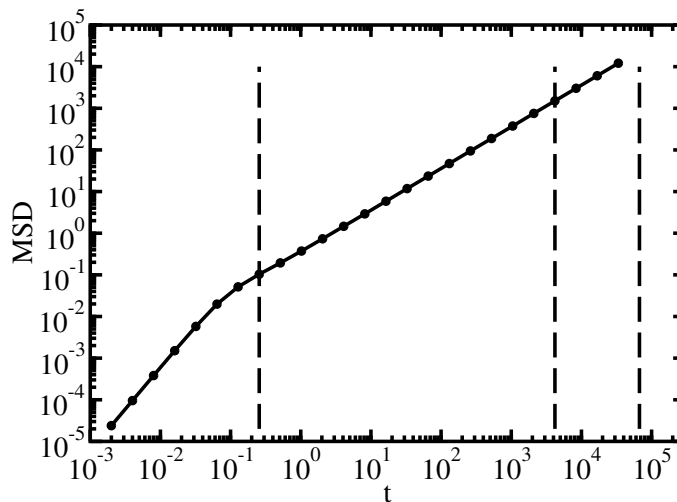


FIG. A1. Time scales associated with the number of steps reported in Table 1. From left to right the vertical dashed lines correspond to how frequently the average value of the force is saved ("Saving" in Table 1) and the length of the short and the long simulations, respectively.

TABLE I. Simulation details.

Interpolation	N	Time step	Short sim	Long sim	Density	Ref. Temp.	Saving
LJ $\rightarrow$ WCA	4096	0.002	$2^{21}$	$2^{25}$	1.0	2.00	128
LJ $\rightarrow$ IPL	4096	0.002	$2^{21}$	$2^{25}$	1.0	2.00	128
YK $\rightarrow$ YK	4096	0.010	$2^{20}$	$2^{24}$	0.5	0.02	128
KA $\rightarrow$ mBLJ	4000	0.005	$2^{24}$	$2^{28}$	1.2	0.48	64

### Comparing the dynamics of KA systems with different cutoffs

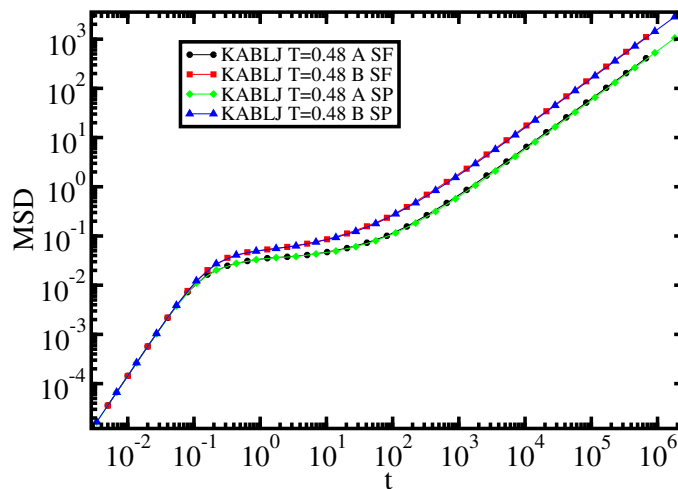


FIG. A2. Comparing the A and B particle MSD of the standard KA systems with shifted-potential (SP) and shifted-force (SF) cutoffs at the state point  $(\rho, T) = (1.2, 0.48)$ .

Figure A2 compares the MSD of the KA system when the interaction potential is truncated by either shifted-force (SF) or shifted-potential (SP) cutoffs at the same (standard) distances. Both the A and B particle MSDs are shown. There is no visible difference between the two cutoff implementations.

### The reduced-force-matching procedure

The reduced-force-matched temperatures (Fig. 6) were calculated by matching the value of the reduced force according to Eq. (6) [34]. The first step is to equilibrate the  $\lambda = 0$  system and simulate it for the number of steps indicated as "Long sim" in Table I. From this the value of the length of the  $3N$ -dimensional force vector  $|\mathbf{F}(\mathbf{R})|$  is sampled with the frequency indicated by "Saving". The time average of the length of the reduced force vector,  $|\mathbf{F}(\mathbf{R})|/k_B T$ , is evaluated and used in the following steps as reference (note that the reduced force vector in general includes a density factor [20], which for simplicity is omitted in this paper because density is kept constant).

The temperature corresponding to the same reduced-force vector at a new value of  $\lambda$  is found using the following iterative procedure.

1. The length of the reduced force vector is evaluated for the new value of  $\lambda$ .
2. A new temperature,  $T(\lambda)$ , is found from  $|\mathbf{F}(\mathbf{R})|_{\lambda}/k_B T(\lambda) = |\mathbf{F}(\mathbf{R})|_{\lambda=0}/k_B T(\lambda = 0)$ .
3. A new simulation of length "Short sim" is run at  $T(\lambda)$ , after which the length of the reduced-force vector is evaluated and compared to the reference value  $|\mathbf{F}(\mathbf{R})|_{\lambda=0}/k_B T(\lambda = 0)$ .
4. Steps 2 and 3 are repeated until the relative difference between the lengths of the reduced force vector is below  $5 \cdot 10^{-6}$ .

The need for this iterative procedure arises from the fact that the theory is only approximate. For selected values of  $\lambda$  (0.2, 0.4, 0.6, 0.8, 1.0) a longer simulation (of "Long sim" steps) is run to obtain better statistic on the RDF and the MSD; these data are the ones shown in the figures of the main paper. The  $\lambda$  parameter varies in all cases between 0 and 1, an interval that is divided into steps of 0.05. This is why there are 21 points for  $T(\lambda)$  in Fig. 6 (short simulations) and only 6 for  $\bar{D}(\lambda)$  (long simulations).

- 
- [1] J. A. Barker and D. Henderson, "What is "liquid"? Understanding the states of matter," *Rev. Mod. Phys.* **48**, 587–671 (1976).
- [2] J.-P. Hansen and I. R. McDonald, *Theory of Simple Liquids: With Applications to Soft Matter*, 4th ed. (Academic, New York, 2013).
- [3] Y. Rosenfeld, "A quasi-universal scaling law for atomic transport in simple fluids," *J. Phys.: Condens. Matter* **11**, 5415–5427 (1999).
- [4] T. Young and H. C. Andersen, "A scaling principle for the dynamics of density fluctuations in atomic liquids," *J. Chem. Phys.* **118**, 3447–3450 (2003).
- [5] T. Young and H. C. Andersen, "Tests of an approximate scaling principle for dynamics of classical fluids," *J. Phys. Chem. B* **109**, 2985–2994 (2005).
- [6] D. M. Heyes and A. C. Branka, "Physical properties of soft repulsive particle fluids," *Phys. Chem. Chem. Phys.* **9**, 5570–5575 (2007).
- [7] P. E. Ramirez-Gonzalez, L. Lopez-Flores, H. Acuna-Campa, and M. Medina-Noyola, "Density-temperature-softness scaling of the dynamics of glass-forming soft-sphere liquids," *Phys. Rev. Lett.* **107**, 155701 (2011).
- [8] M. Schmiedeberg, T. K. Haxton, S. R. Nagel, and A. J. Liu, "Mapping the Glassy Dynamics of Soft Spheres onto Hard-Sphere Behavior," *EPL* **96**, 36010 (2011).
- [9] L. Lopez-Flores, H. Ruiz-Estrada, M. Chavez-Paez, and M. Medina-Noyola, "Dynamic Equivalences in the Hard-Sphere Dynamic Universality Class," *Phys. Rev. E* **88**, 042301 (2013).
- [10] J. C. Dyre, "Simple liquids' quasiuniversality and the hard-sphere paradigm," *J. Phys. Condens. Matter* **28**, 323001 (2016).
- [11] L. Verlet, "Computer "experiments" on classical fluids. II. Equilibrium correlation functions," *Phys. Rev.* **165**, 201–214 (1968).
- [12] J. D. Weeks, D. Chandler, and H. C. Andersen, "Role of repulsive forces in determining the equilibrium structure of simple liquids," *J. Chem. Phys.* **54**, 5237–5247 (1971).
- [13] J. H. Dymond, "Hard-sphere theories of transport properties," *Chem. Soc. Rev.* **14**, 317–356 (1985).
- [14] G. N. Sarkisov, "Approximate equations of the theory of liquids in the statistical thermodynamics of classical liquid systems," *Physics Uspekhi* **42**, 545–561 (1999).
- [15] J.-M. Bomont, "Recent advances in the field of integral equation theories: Bridge functions and applications to classical fluids," *Adv. Chem. Phys.* **139**, 1–83 (2008).
- [16] S. Zhou and J. R. Solana, "Progress in the perturbation approach in fluid and fluid-related theories," *Chem. Rev.* **109**, 2829–2958 (2009).
- [17] N. E. Dubinin, N. A. Vatolin, and V. V. Filippov, "Thermodynamic perturbation theory in studies of metal melts," *Russ. Chem. Rev.* **83**, 987–1002 (2014).
- [18] Y. Rosenfeld, "Relation between the transport coefficients and the internal entropy of simple systems," *Phys. Rev. A* **15**, 2545–2549 (1977).
- [19] A. K. Bacher, T. B. Schröder, and J. C. Dyre, "Explaining why simple liquids are quasi-universal," *Nat. Commun.* **5**, 5424 (2014).
- [20] N. Gnan, T. B. Schröder, U. R. Pedersen, N. P. Bailey, and J. C. Dyre, "Pressure-energy correlations in liquids. IV. "Isomorphs" in liquid phase diagrams," *J. Chem. Phys.* **131**, 234504 (2009).
- [21] J. C. Dyre, "Hidden scale invariance in condensed matter," *J. Phys. Chem. B* **118**, 10007–10024 (2014).
- [22] J. C. Dyre, "Perspective: Excess-entropy scaling," *J. Chem. Phys.* **149**, 210901 (2018).
- [23] A. K. Bacher, T. B. Schröder, and J. C. Dyre, "The EXP pair-potential system. II. Fluid phase isomorphs," *J. Chem. Phys.* **149**, 114502 (2018).
- [24] J. C. Dyre, "NVU perspective on simple liquids' quasiuniversality," *Phys. Rev. E* **87**, 022106 (2013).
- [25] T. S. Ingebrigtsen, S. Toxvaerd, O. J. Heilmann, T. B. Schröder, and J. C. Dyre, "NVU dynamics. I. Geodesic motion on the constant-potential-energy hypersurface," *J. Chem. Phys.* **135**, 104101 (2011).
- [26] T. S. Ingebrigtsen, S. Toxvaerd, T. B. Schröder, and J. C. Dyre, "NVU dynamics. II. Comparing to four other dynamics," *J. Chem. Phys.* **135**, 104102 (2011).
- [27] D. Lang, L. Costigliola, and J. C. Dyre, "NVU view on energy polydisperse Lennard-Jones systems," *Phys. Rev. E* **111**, 025420 (2025).
- [28] M. E. Fisher and D. Ruelle, "The stability of many-particle systems," *J. Math. Phys.* **7**, 260–270 (1966).
- [29] D. M. Heyes and G. Rickayzen, "The stability of many-body systems," *J. Phys. Condens. Matter* **19**, 416101 (2007).
- [30] T. B. Schröder and J. C. Dyre, "Simplicity of condensed matter at its core: Generic definition of a Roskilde-simple system," *J. Chem. Phys.* **141**, 204502 (2014).
- [31] L. D. Landau and E. M. Lifshitz, *Statistical Physics [Eq. (33.14)]* (Pergamon, Oxford, 1958).
- [32] H. H. Rugh, "Dynamical approach to temperature," *Phys. Rev. Lett.* **78**, 772–774 (1997).
- [33] J. G. Powles, G. Rickayzen, and D. M. Heyes, "Temperatures: old, new and middle aged," *Mol. Phys.* **103**, 1361–1373 (2005).
- [34] T. B. Schröder, "Predicting scaling properties from a single fluid configuration," *Phys. Rev. Lett.* **129**, 245501 (2022).
- [35] J. E. Lennard-Jones, "On the determination of molecular fields. I. From the variation of the viscosity of a gas with temperature," *Proc. R. Soc. London A* **106**, 441–462 (1924).
- [36] W. G. Hoover, S. G. Gray, and K. W. Johnson, "Thermodynamic properties of the fluid and solid phases for inverse power

- potentials,” *J. Chem. Phys.* **55**, 1128–1136 (1971).
- [37] A. C. Branka and D. M. Heyes, “Thermodynamic properties of inverse power fluids,” *Phys. Rev. E* **74**, 031202 (2006).
- [38] D. M. Heyes and A. C. Branka, “Self-diffusion coefficients and shear viscosity of inverse power fluids: from hard- to soft-spheres,” *Phys. Chem. Chem. Phys.* **10**, 4036–4044 (2008).
- [39] H. Yukawa, “On the interaction of elementary particles. I,” *Proc. Phys. Math. Soc. Jpn.* **17**, 48–57 (1935).
- [40] N. P. Bailey, T. S. Ingebrigtsen, J. S. Hansen, A. A. Veldhorst, L. Bøhling, C. A. Lemarchand, A. E. Olsen, A. K. Bacher, L. Costigliola, U. R. Pedersen, H. Larsen, J. C. Dyre, and T. B. Schröder, “RUMD: A general purpose molecular dynamics package optimized to utilize GPU hardware down to a few thousand particles,” *Scipost Phys.* **3**, 038 (2017).
- [41] M. P. Allen and D. J. Tildesley, *Computer Simulation of Liquids* (Oxford Science Publications (Oxford), 1987).
- [42] W. Kob and H. C. Andersen, “Testing Mode-Coupling Theory for a Supercooled Binary Lennard-Jones Mixture I: The van Hove Correlation Function,” *Phys. Rev. E* **51**, 4626–4641 (1995).
- [43] W. Kob and H. C. Andersen, “Testing mode-coupling theory for a supercooled binary Lennard-Jones mixture I: The van Hove correlation function,” *Phys. Rev. E* **51**, 4626–4641 (1995).
- [44] U. R. Pedersen, T. B. Schröder, and J. C. Dyre, “Phase diagram of Kob-Andersen-type binary Lennard-Jones mixtures,” *Phys. Rev. Lett.* **120**, 165501 (2018).
- [45] S. Franz, R. Mulet, and G. Parisi, “Kob-Andersen model: A nonstandard mechanism for the glassy transition,” *Phys. Rev. E* **65**, 021506 (2002).
- [46] Peter Crowther, Francesco Turci, and C. Patrick Royall, “The nature of geometric frustration in the Kob-Andersen mixture,” *J. Chem. Phys.* **143**, 044503 (2015).
- [47] D. Coslovich, M. Ozawa, and W. Kob, “Dynamic and thermodynamic crossover scenarios in the Kob-Andersen mixture: Insights from multi-CPU and multi-GPU simulations,” *Eur. Phys. J. E* **41**, 62 (2018).
- [48] T. B. Schröder and J. C. Dyre, “Solid-like mean-square displacement in glass-forming liquids,” *J. Chem. Phys.* **152**, 141101 (2020).
- [49] S. Toxvaerd and J. C. Dyre, “Communication: Shifted forces in molecular dynamics,” *J. Chem. Phys.* **134**, 081102 (2011).
- [50] T. S. Ingebrigtsen and J. C. Dyre, “*NVU* dynamics. III. Simulating molecules,” *J. Chem. Phys.* **137**, 244101 (2012).
- [51] J. Lützen, *Mechanistic Images in Geometric Form: Heinrich Hertz’s “Principles of Mechanics”* (Oxford University Press, Oxford, 2005).